Available online at www.sciencedirect.com
ScienceDirect
Journal of Power Sources 158 (2006) 1386–1393
JOURNAL OF POWER SOURCES
www.elsevier.com/locate/jpowsour

Effect of an electrolyte salt dissolving in polysiloxane-based electrolyte on passive film formation on a graphite electrode

Hiroshi Nakahara [a,*], Steven Nutt [b]

[a] *Quallion LLC, Sylmar Biomedical Park, 12744 San Fernando Rd., Sylmar, CA 91342, USA*
[b] *Department of Material Science and Engineering, University of Southern California, Los Angeles, CA 90089-0241, USA*

Received 28 September 2005; received in revised form 14 October 2005; accepted 14 October 2005
Available online 21 November 2005

Abstract

Electrochemical impedance spectroscopy (EIS) was performed during the first charge of a graphite/lithium metal test cell to determine the effect of an electrolyte salt on passive film formation in a polysiloxane-based electrolyte. The graphite electrode was separated from the lithium metal electrode by a porous polyethylene membrane immersed in a polysiloxane-based electrolyte with the dissolved lithium bis(oxalato) borate (LiBOB) or lithium bis(trifluoromethanesulfonyl) imide (LiTFSI). In case of LiTFSI, the conductivity of system decreased at 1.2 V. In contrast, for the case of LiBOB, the conductivity decreased at 1.7 V. The magnitudes of charge transfer resistance and film resistance for LiTFSI were smaller than that for LiBOB. Passive films on highly oriented pyrolytic graphite (HOPG) after charging (lithiating) in polysiloxane-based electrolyte were inspected microscopically. Gel-like film and island-like films were observed for LiBOB [H. Nakahara, A. Masias, S.Y. Yoon, T. Koike, K. Takeya, Proceedings of the 41st Power Sources Conference, vol. 165, Philadelphia, June 14–17, 2004; H. Nakahara, S.Y. Yoon, T. Piao, S. Nutt, F. Mansfeld, J. Power Sources, in press; H. Nakahara, S.Y. Yoon, S. Nutt, J. Power Sources, in press]. However, for LiTFSI, there was sludge accumulation on the HOPG surface. Compositional analysis revealed the presence of silicon on both HOPG specimens with LiBOB and with LiTFSI. The electrolyte salt dissolved in the polysiloxane-based electrolyte changed the electrochemical and morphological nature of passive films on graphite electrode.

Keywords: Lithium battery; Graphite; Siloxane; LiTFSI; Passive film

1. Introduction

Past research has focused on the formation of the solid electrolyte interface (SEI) on the graphite electrode surface in non-aqueous electrolytes, such as the ethylene carbonate/diethyl carbonate system [4,5]. In recent reports, the authors determined that exfoliation of graphene layers occurred during initial charging in propylene carbonate-based electrolytes because of co-intercalation of solvent [4,6]. Earlier studies asserted that the SEI film formed mainly by a solvent decomposition reaction, and that it was composed of $ROCO_2Li$ species, Li_2CO_3, and LiF [7–10]. Investigators concluded that the novel lithium salt, lithium bis(oxalato) borate (LiBOB), forms an SEI film directly on graphite, rather than by a solvent decomposition reaction [11–13].

Polysiloxane-based (PS-B) electrolyte is considered to be suitable for a lithium battery system because of the high conductivity relative to other polymer materials [14–18]. Polyethylene oxide (PEO) is a well-known solid polymer electrolyte that shows conductivity in the range of 10^{-6} to 10^{-7} S cm^{-1} [14–18], while the conductivity of the PS-B electrolyte exceeds a value of approximately 10^{-3} S cm^{-1} [19]. Thus, the PS-B electrolyte has emerged as a prime candidate for the development of large lithium batteries for applications such as electric vehicles, in which safety is a prime consideration [19].

In recent work, SEI formation on graphite surfaces in a PS-B electrolyte was investigated [1–3]. The existence of two types of passive film and the associated morphological features was revealed by SEM observations [1]. One passive film was island-like and formed directly on the graphite surface, while the other was a gel-like film covering the island-like film [1]. Electrochemical impedance spectroscopy (EIS) for the graphite/lithium cell with the PS-B electrolyte containing LiBOB revealed that the electrochemical functions of passive films depended on cell

* Corresponding author. Tel.: +1 818 833 2000; fax: +1 818 833 2001.
E-mail address: hiroshi@quallion.com (H. Nakahara).

0378-7753/$ – see front matter © 2005 Elsevier B.V. All rights reserved.
doi:10.1016/j.jpowsour.2005.10.042

voltage. The magnitudes of the film resistance and the charge transfer resistance were much larger than those of conventional carbonate-based electrolytes [2,3]. Furthermore, the addition of vinyl ethylene carbonate (VEC) to PS-B electrolytes increased the discharge capacity of the graphite electrode and inhibited gel-like film formation causing decrease of film resistance and charge transfer resistance [1,3]. These reports suggested that the electrochemical and morphological characteristics of passive films on the graphite electrode charged in PS-B electrolytes could be modified by optimizing the electrolyte components for commercialization.

An electrolyte salt can be used to modify the passive films on graphite electrode [20–25]. Generally, an electrolyte salt having a large anion is chosen to facilitate anion–cation dissociation, and thus obtain high lithium conductivity. A variety of lithium salts have been developed to provide charge carriers for current flow in lithium cells, including lithium hexafluorophosphate ($LiPF_6$), lithium tetrafluoroborate ($LiBF_4$), lithium perchlorate ($LiClO_4$), lithium hexafluoroarsenate ($LiAsF_6$), lithium trifluoromethylsulfate ($LiCF_3SO_3$), LiBOB ($LiB(C_2H_4COO)_2$), and LiTFSI ($LiN(SO_2CF_3)_2$) [20–22,25]. $LiCF_3SO_3$ and LiTFSI were developed specifically for polymer electrolyte systems because the large size and partly delocalized charge of the anions inhibits the formation of ion pairs and increases the transport number of lithium ion [20]. In addition, when used as an electrolyte salt, LiTFSI produced the most thermally stable lithium-intercalated graphite [22]. LiTFSI is a strong candidate for development of polymer electrolytes for lithium battery systems.

In this study, a PS-B electrolyte containing LiTFSI was used to explore the effect of an electrolyte salt on the passive film formation on graphite electrode. We hypothesized that passive film formation could be suppressed by substituting LiTFSI for LiBOB, because LiBOB is more reductive-decomposed than LiTFSI [11–13,22]. An electrolyte salt was designed expressly for the PS-B electrolyte. In addition, experiments were conducted to clarify the contribution of the electrolyte salt to the passive film formation. Furthermore, LiTFSI was selected as a suitable salt for the PS-B electrolyte because it was originally developed for polymer electrolytes. This substitution would reduce film resistance and improve the electrochemical performance of a graphite electrode–lithium battery. The surface morphology of HOPG was examined after charging in a PS-B electrolyte containing dissolved LiTFSI, and EIS was performed to assess the change in electrochemical characteristics of passive films on the graphite electrode. The results were compared with those for LiBOB [2].

2. Experimental

2.1. Electrode morphology and composition

A polysiloxane-based electrolyte containing dissolved LiTFSI was used to modify the surface of HOPG (2 mm × 2 mm × 1 mm), and LiBOB was also used as a control salt for the electrolyte. A block of HOPG was used as the working electrode, and copper mesh was wrapped around the HOPG block to function as a current collector. The electrode was covered with a polyethylene porous separator, and lithium metal was pressed against a copper mesh and used as the counter electrode. The working electrode, counter electrode, separator, and electrolyte were packaged in a heat-sealed aluminum laminated bag. The laminated cell was charged to 0.02 V at 25 °C. The charged electrode was removed from the disassembled cell in a glove box filled with Ar gas while maintaining the dew-point below −75 °C, then rinsed with diethyl carbonate (DEC), and dried under vacuum at room temperature. The surfaces of the HOPG were examined by SEM (JEOL JSM-5910LV) after sputter-coating with gold. In addition, the composition of specimens was analyzed using energy dispersive X-ray spectroscopy (EDX: Oxford Instruments, EDS INCAEnergy 7274).

2.2. Electrochemical impedance spectroscopy

The graphite electrodes were prepared by mixing 33.6 g of mesocarbon microbeads (Osaka Gas Co., Ltd., MCMB 25–28), 14.4 g of graphite fiber (Petoca Co., Ltd., GMCF), 62.6 g of 2 wt% aqueous solution of carboxymethyl cellulose (Dai-ichi Kogyo Seiyaku Co., Ltd., Celogen WSC), and 1.88 g of a 40% aqueous dispersion of styrene butadiene rubber (Dai-ichi Kogyo Seiyaku Co., Ltd., BM-400) in a mixer. The mixture was spread on a copper foil (10 μm thick) with a doctor blade and dried in an oven at 80 °C. The dried electrode plate was then pressed by using a roll press to a thickness of 102 μm. Pressed electrodes were dried in a vacuum oven at 120 °C for 12 h. The carbonaceous electrodes (15 mm in diameter) were punched out of the dried electrode plate. Lithium metal electrodes (16 mm in diameter) were punched from a lithium metal sheet (Honjo metal, 100 μm thick). Coin cells (2032-type) were prepared by stacking a lithium metal electrode, a separator, a carbonaceous electrode, spacer disks made from stainless steel, and a spring in sequence. The separator was a 25 μm-thick polyethylene porous membrane (Tonen Chemical Co., Ltd.). The molecular structure of poly(dimethyl) siloxane poly(ethylene oxide) (PMSEO) investigated in this study is shown in Fig. 1. In the present experiments, the molecule indexed at $m = 0$, $n = 8$, and $x = 3$ was used. Lithium bis(oxalato) borate (Chemetall GmbH), was dissolved in PMSEO to achieve a 0.8 M concentration for a control testing. LiTFSI (Morita Chemical Industries Co., Ltd.) was dissolving into PMSEO with 0.8 M concentration as well. The electrolyte was a liquid at room temperature. All parts used for the coin cell assembly were dried in a vacuum oven at 60 °C for more than 8 h.

AC impedance measurements were performed with a potentiostat (Solartron, SI1287) and a transfer function analyzer (Solartron, 1255B). The frequency used for the impedance

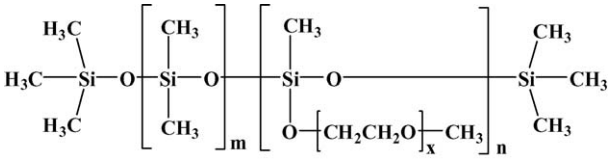

Fig. 1. Molecular structure of poly(dimethyl) siloxane poly(ethylene oxide).

measurements was 50 mHz to 200 kHz, and the signal amplitude was 10 mV. Potential step coulometry was performed with an electrochemical interface (Solartron, SI1287). Impedance spectra were measured after charging the cell had been charged at a rate of C/200 to the prescribed voltage and holding at that voltage for 24 h. The voltage was then stepped to the next potential, and the procedure was repeated. In this manner, the cell was charged from the initial open circuit voltage (OCV) down to 0.05 V at 25 °C. The counter electrode and the reference electrode were lithium metal.

The impedance data were analyzed using commercial software that included a batch fitting function (Scribner Associates, Inc., Zview™). Step-by-step fitting was performed for multiple sets of impedance spectra. By this method, initial values of the electrical components in the equivalent circuit were obtained from values fitted in the previous step. These values were obtained for a set of measured impedance spectra, from which a complex plane plot was generated at a higher voltage. Next, the fitted parameters generated in one step were used as initial values to fit the spectra of the previous step. These procedures were repeated in successive steps until the values of the fit parameters converged [26]. The conductivity of experimental system was calculated using the real part of the impedance obtained in the high-frequency region of the complex plane plot.

3. Implementation of equivalent circuit model

EIS is widely used to investigate electrolyte–electrode interface reactions [27–35] such as the electrochemical lithium intercalation reaction in carbonaceous material within the carbonate electrolyte system and the subsequent formation of SEI films [36–42]. Of particular relevance to the present study are the reports of EIS data for lithium ion cells and lithium metal cells have been reported extensively [28–30,32,43]. These studies highlight the value of analog constructs that afford insight into underlying electrochemical mechanisms.

Logic diagrams and equivalent circuits (ECs) have been proposed for cells with a graphite/lithium metal configuration [44–49]. In most of these studies, an *R–C* parallel or *R*–CPE parallel circuit was used to describe the presence of a surface film layer on the electrode [44,46–50]. The EC represents the electrical properties of the graphite electrode when charged in a PS-B electrolyte (Fig. 2) [2,3]. Segments include (a) electric connection resistance and the electrolyte bulk resistance corresponding to the resistance at the highest frequencies, followed by (b) an *R–C* parallel circuit describing the SEI layer in the middle frequency region, and finally, (c) an *R–C* parallel circuit for double layer capacitance and charge transfer reaction, including a Warburg diffusion term in the low-frequency region corresponding to lithium diffusion in the solid state [36,39,40,47,51].

In general, because the measured semicircles often tend to be depressed in a complex plane plot (as opposed to those generated under ideal experimental conditions), a constant phase element (CPE) is used in an EC for the porous electrode. The use of a CPE is justified because of electrode geometry effects on capacitance

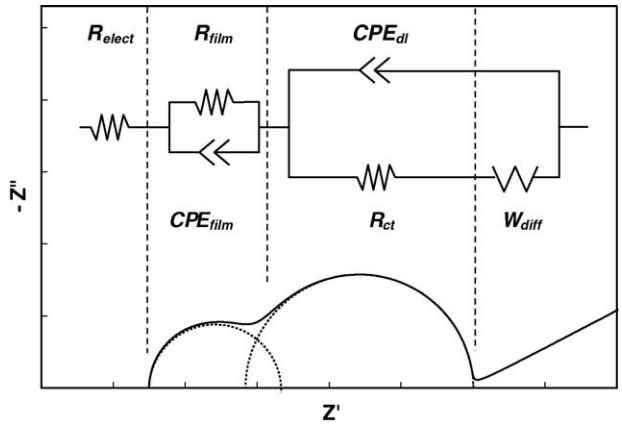

Fig. 2. Equivalent circuit for graphite/polysiloxane based electrolyte/lithium metal cell.

in electrochemical reactions [52–56]. The complex impedance of a CPE, Z_{CPE}, is expressed by:

$$Z_{CPE} = \frac{1}{T(j\omega)^P} \quad (1)$$

where T represents the pseudo-capacitance modified by the electrode geometry, j an imaginary number, and P is an exponential parameter that expresses the electrode geometry as a number. Finally, $\omega = 2\pi f$ is the angular frequency and f is the frequency of the applied AC signal.

Fig. 2 shows the EC with the resistance element, R_{elect}, representing the resistance of the bulk electrolyte including connection resistance in the system, and an *R*–CPE parallel circuit [44–49,57,58] for the passive film with resistance R_{film} and constant phase element, CPE_{film}. The final component is an *R*–CPE parallel element that represents the electric double-layer capacitance as a constant-phase element, CPE_{dl}, and the charge transfer resistance, R_{ct}, representing the site where the electrochemical reaction occurs [59]. Each CPE contains the pseudo-capacitance and the exponential parameter, as expressed in Eq. (1), i.e., T_{film} and P_{film} for CPE_{film}, and T_{dl} and P_{dl} for CPE_{dl}, respectively. The diffusion impedance $W_{s,diff}$ is connected in series to R_{ct} [53,58,60–62].

4. Results

4.1. SEM images and EDX qualitative analysis

SEM images of HOPG revealed clean edges and basal planes (Fig. 3a and b, respectively). When using LiBOB as an electrolyte salt, island-like and gel-like films were observed (Fig. 3c and d) [1,2]. The gel-like film covered the island-like film on the HOPG surface, and the island-like film was occasionally exposed where the gel-like film had ruptured (Fig. 3d) [1,2]. When using LiTFSI as an electrolyte salt, films were deposited that resembled the gel-like film in Fig. 3e and f. However, unlike the gel-like film shown in Fig. 3d, which was a continuous sheet of constant thickness, the deposit was an aggregate sludge. This was confirmed by re-examining the specimen after scratching the HOPG surface with tweezers. Trace amounts of

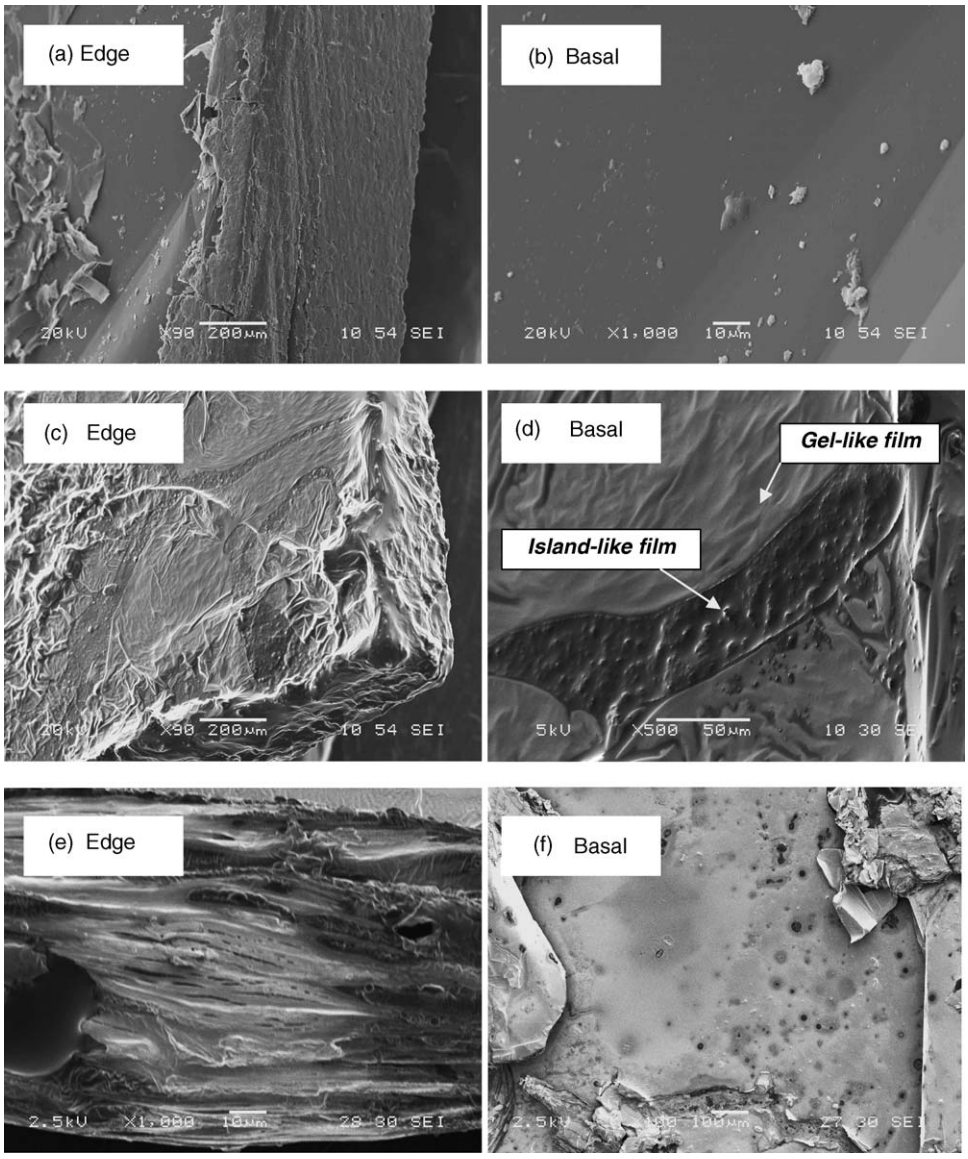

Fig. 3. SEM images of HOPG block charged at 0.02 V vs. Li/Li$^+$, (a and b) before charging, (c and d) after charging in polysiloxane-based electrolyte containing LiBOB (taken from ref. [2]), and (e and f) LiTFSI.

silicon were detected in both HOPG samples charged in the PS-B electrolyte—one with LiBOB and one with LiTFSI. (Silicon is present in the polysiloxane.)

4.2. EIS results

The EIS data measured at 2.5, 1.7, 0.4, and 0.05 V are plotted in Fig. 4. The complex plane plots for PS-B electrolyte with LiBOB and for PS-B electrolyte with LiTFSI are shown in Fig. 4a and b, respectively. The semicircles in the complex plane plots are depressed and consist of multiple semicircles. The semicircle in the mid- or low-frequency region became significantly broader as the cell voltage was decreased. Use of LiTFSI in place of LiBOB caused a smaller semicircle diameter. As the applied voltage was decreased, the straight line in the low frequency region became shorter, and an additional semicircle was detected.

Fig. 5 shows Bode plots corresponding to the complex plane plots in Fig. 4b (for PS-B electrolyte with LiTFSI). The upper figure (Fig. 5a) shows the logarithm of the measured impedance modulus, $|Z|$, plotted against the logarithm of the applied frequency. The impedance modulus decreased with decreasing cell voltage, in contrast to the case of using LiBOB as an electrolyte salt (not shown) [2]. The lower figure (Fig. 5b) shows the phase angle of the measured impedance plotted against the applied frequency. The phase angle decreased with decreasing cell voltage in the frequency range below $10^{4.5}$ Hz. The magnitude of the phase angle was larger at lower frequencies.

All impedance elements of the EC depended on the cell voltage, as shown in Fig. 6, where cell conductivity, derived using the experimental value of R_{elect}, is plotted versus voltage. The R_{elect} includes electrolyte conductivity, and electric contact conductivity among graphite particles in the electrode and among

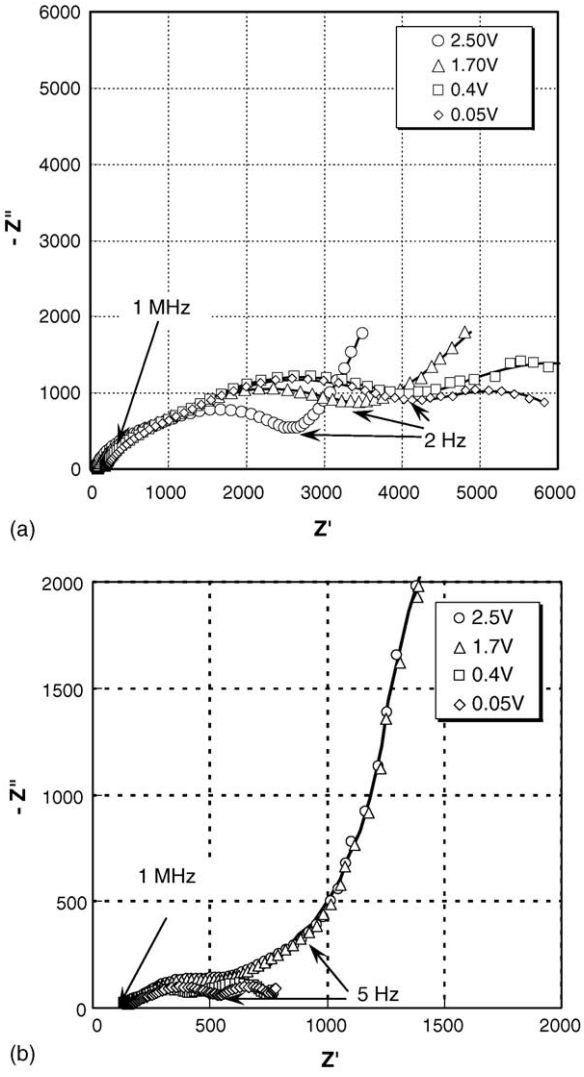

Fig. 4. Nyquist plots for graphite/polysiloxane based electrolyte/lithium metal cell measured at 2.5, 1.7, 0.4, and 0.05 V vs. Li/Li$^+$, (a) LiBOB and (b) LiTFSI.

cell parts. The R_{elect} for LiTFSI was constant in the voltage range above 1.2 V and below 1.0 V, but changed significantly between 1.0 and 1.2 V. In contrast, the R_{elect} for LiBOB was approximately constant between 2.1 and 3.2 V, but decreased sharply with decreasing cell voltage between 1.6 and 1.9 V, then decreased more gradually in the ranges of 1.05–1.2 and 0.3–0.5 V. The data indicate that the change in R_{elect} with cell voltage is significantly affected by the type of electrolyte salt.

The circuit parameters corresponding to the passive films were evaluated to clarify the dependence on cell-voltage. For example, the dependence of R_{film} on cell voltage is shown in Fig. 7. The magnitude of the R_{film} for LiTFSI was hundreds of ohms less than for LiBOB. The R_{film} for electrolyte with LiTFSI was constant at voltages above 1.3 V, and increased between 1.0 and 1.2 V, and did not change significantly between 0.5 and 1.2 V. On the other hand, the R_{film} for electrolyte with LiBOB was constant at voltages above 1.8 V, and increased between 1.5–1.8, 1.2–1.3 and 0.3–0.5 V. R_{film} for both electrolytes decreased below 0.5 V.

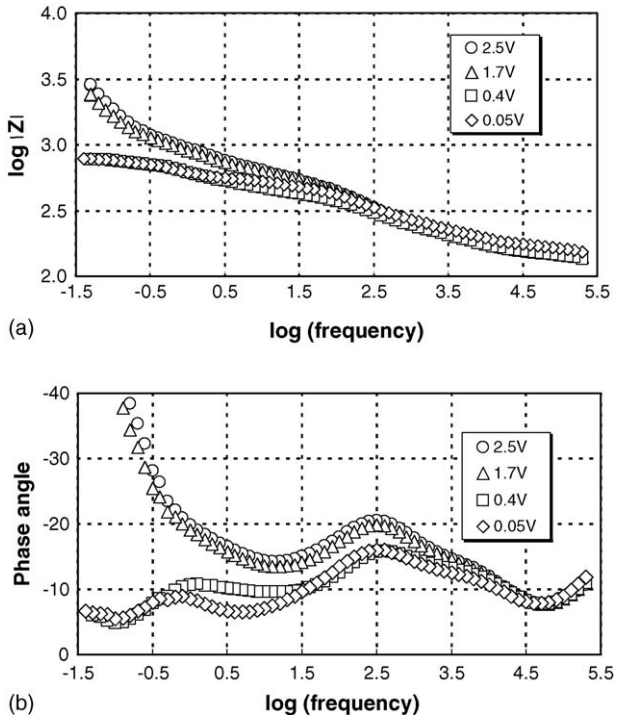

Fig. 5. (a and b) Bode plots for graphite/polysiloxane based electrolyte with LiTFSI/lithium metal cell measured at 2.5, 1.7, 0.4, and 0.05 V vs. Li/Li$^+$.

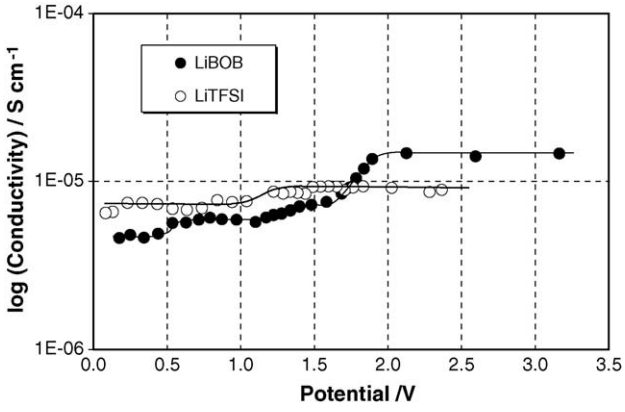

Fig. 6. The calculated conductivity as a function of the cell voltage.

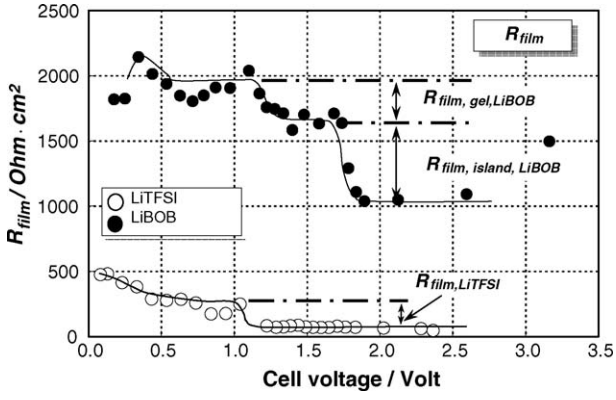

Fig. 7. Values of R_{film} as a function of the voltage of the graphite/polysiloxane based electrolyte/lithium metal cell.

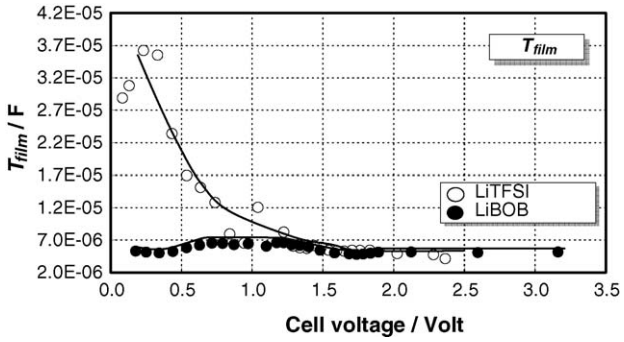

Fig. 8. Values of T_{film} as a function of the voltage of graphite/polysiloxane based electrolyte/lithium metal cell.

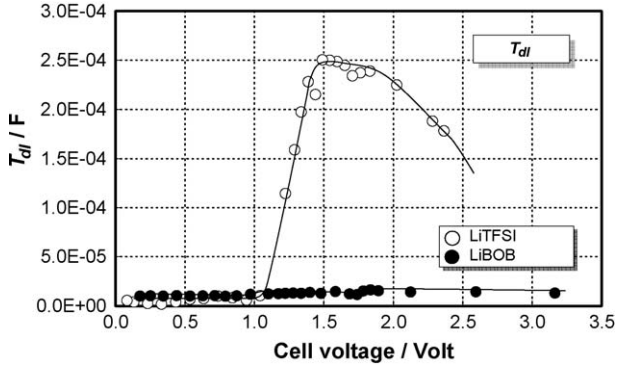

Fig. 9. Values of T_{dl} as a function of the voltage of graphite/polysiloxane based electrolyte/lithium metal cell.

While the T_{film} values for electrolyte with LiBOB showed an increase in the voltage range of 1.2–1.7 V and a decrease at 0.4–0.6 V, the T_{film} for electrolyte with LiTFSI showed a constant value in the range above 1.7 V, followed by a monotonic increase below 1.7 V with decrease of cell voltage (Fig. 8). The values of the double layer capacitance parameter, T_{dl}, for the electrolyte with LiTFSI were an order of magnitude larger than that with LiBOB (Fig. 9). The T_{dl} for both electrolytes did not change above 1.75 V, and decreased with decreasing cell voltage between 1.4 and 1.75 V.

The dependence of the charge transfer resistance, R_{ct}, on the cell voltage is shown in Fig. 10. The value of R_{ct} for both electrolytes was constant above 1.9 V. The R_{ct} for LiTFSI was 2650 Ω cm^2 less than the one for LiBOB. While the R_{ct} for LiBOB increased with decreasing cell voltage below 1.9 V. In contrast, R_{ct} for LiTFSI decreased between 1.0 and 1.4 V and was constant below 1.0 V. The R_{ct} for LiTFSI was 6500 Ω cm^2 less than the one for LiBOB. The interpretation of these disparate values is included in the following section.

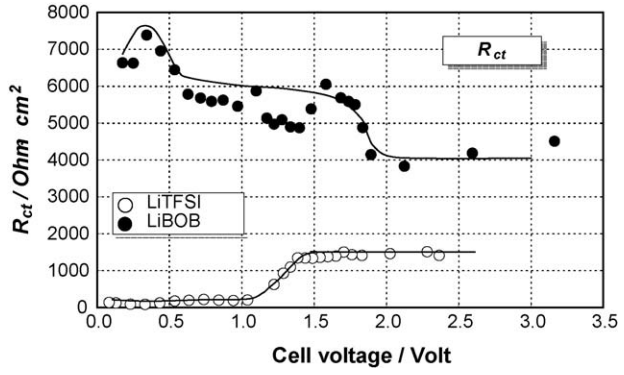

Fig. 10. Values of R_{ct} as a function of the voltage of graphite/polysiloxane based electrolyte/lithium metal cell.

5. Discussion

Earlier work revealed the morphological, compositional and electrochemical changes in the graphite electrode surface charged in PS-B electrolyte containing LiBOB [1–3]. Formation of island-like film and gel-like films was initiated by the decomposition of bis(oxalato) borate anion during the 1st charge of a graphite electrode [2,3]. The modification of these passive films was carried out by VEC addition to the PS-B electrolyte, which prevented the gel-like film formation. These results led to expectations of improvement in PS-B electrolyte and the prospect for commercialization in the lithium battery industry [3]. In particular, the results indicated the benefit of reducing both R_{film} and R_{ct} [2,3]. The present investigation has shown that this can be achieved by the judicious selection of electrolyte salt, as opposed to the use of additives such as VEC.

The complex plane plots shown in Fig. 4a and b indicate that the curves calculated using the fit parameters from the proposed EC accurately match the experimental data (shown with markers). The small uncertainty, χ^2, of the fitting supports the assertion that the proposed EC (Fig. 2) is suitable for modeling the electrochemical reactions in the graphite/PS-B electrolyte/lithium metal cell system, both with LiBOB and with LiTFSI. The EC thus constitutes a reliable analog representing the electrochemical properties of the passive films and the electrochemical reaction on the graphite surface.

The two salts considered in these experiments yielded several similar observations. For example, the values of R_{film} for both LiTFSI and LiBOB changed at 1.2 V. The R_{film}, *increment* for LiTFSI was 180 Ω cm^2, while the $R_{film,gel}$ *increment* for LiBOB was 265 Ω cm^2. In addition, the following similarities for both LiTFSI and LiBOB samples were noted, including (a) the change in R_{film} occurred at the same voltage, (b) the magnitude of increase in R_{film} was similar ($R_{film,LiTFSI}$ and $R_{film,gel,LiBOB}$ in Fig. 7), (c) the onset of gel-like film formation occurred at 1.2 V [1], and (d) Si was detected in the substance on the HOPG surface. These similarities indicate that the polysiloxane molecule may be decomposed at 1.2 V, because the polysiloxane molecule is inherently susceptible to reduction. For the LiTFSI salt, the decomposition products of the polysiloxane molecules produced a sludge-like deposit (Fig. 3f), as opposed to a smooth continuous film (Fig. 3c and d). This supports our hypothesis that the LiBOB decomposition product induces cross-linking in the polysiloxane decomposition product and generates the gel-like substance [1–3]. The gel-like film is therefore formed through the result of a synergetic reaction involving decomposition of both LiBOB and polysiloxane molecules.

Previous reports have shown that the reduction decomposition of LiTFSI on graphite surfaces produces LiF, C_2F_xLi, LiS_2O_4, and Li_3N [23,24], any or all of which may constitute

part of the sludge deposit observed in the present work. All of these substances are ionic compounds and, unlike LiBOB in PS-B electrolyte, do not form cross-links for polysiloxane molecules [1,2,11–13]. The ionic compounds noted here were produced in small quantities [22,25]. Consequently, while any LiTFSI decomposition associated with sludge formation might be expected to cause a corresponding change in $R_{film,LiTFSI}$, no such change was detected. Nevertheless, products from decomposition of polysiloxane molecules might dissolve into the electrolyte, causing the decrease in electrolyte conductivity observed at 1.2 V. However, it is considered that most of part in the decrease of conductivity was attributed to the electric contact resistance among graphite particles due to the passive film formations, because the voltage at which the conductivity decreased corresponds to sludge formation.

The R_{ct} for LiTFSI (79 $\Omega\,cm^2$) was two orders of magnitude less than R_{ct} for LiBOB (7418 $\Omega\,cm^2$) in the voltage range below ~0.5 V (which, incidentally, is the potential of the graphite electrode used in practical operation of a lithium battery). The value of $R_{ct,LiTFSI}$ (79 $\Omega\,cm^2$) was comparable to the R_{ct} for conventional carbonate-based electrolytes, such as those containing $LiPF_6$ (3–10 $\Omega\,cm^2$ [40]) and $LiClO_4$ (60–80 $\Omega\,cm^2$ [44]). The charge transfer reaction occurred at the graphite–passive film boundary. The passive film is the solid state electrolyte that conducts lithium ions. The decrease in $R_{ct,LiTFSI}$ corresponds to the change in $R_{film,LiTFSI}$. Hence, the sludge-like deposition formed by the decomposition of polysiloxane molecules is likely to enhance the formation of a charge transfer complex. Lithium ions intercalated in graphite are assumed to remain ions [63,64]. The charge transfer complex is therefore the lithium ion desolvated from the anions in the solid state electrolyte (passive film). On the other hand, the island-like film decomposed with LiBOB does not form such a complex. Hence, the difference between $R_{ct,LiTFSI}$ and $R_{ct,LiBOB}$ is attributed to the complex arising from the solvation interaction between lithium ions and anions in the solid state electrolyte. We assert that in order to improve the characteristics of a graphite electrode for lithium batteries, it is necessary to prevent the formation of the gel-like film and also to modify the composition of the passive film depositing directly on graphite surface. The small value of $R_{ct,LiTFSI}$ improves the high discharge rate capability and low temperature discharge capability of the graphite electrode in a lithium battery.

6. Conclusions

The characteristics of the passive surface film on a graphite electrode were altered by the type of electrolyte salts contained in a PS-B electrolyte. The use of LiTFSI salt produced a sludge-like Si-bearing deposit on the graphite surface instead of the island-like or gel-like films formed with LiBOB. In addition, the charge transfer resistance and passive film resistance decreased and were comparable to the resistance values in conventional carbonate electrolyte systems. However, in practical lithium batteries, LiTFSI can corrode the aluminum positive current collector [65,66], which constitutes a significant barrier to the commercialization of PS-B electrolytes. The results presented here dictate that practical battery design must involve selection of an electrolyte salt suitable for use in the PS-B electrolyte system. Such salts significantly modify the nature of the passive film, and thus will affect the electrochemical performance of a graphite electrode in lithium batteries [1–3,67].

The results in this study highlight the possibility of using LiTFSI as an electrolyte salt for PS-B electrolytes to achieve performance superior to LiBOB. At the same time, the results also indicate the poor resistance of the polysiloxane molecule against reduction decomposition, suggesting the need to optimize the polysiloxane molecular structure for resistance against reducing environments. To realize this, the polysiloxane molecular structures reported here will require optimization, which may be achieved through surface modification of the graphite electrode. Microscopic observations and EIS analysis of structural variants of polysiloxane should provide further insight into the nature and formation mechanisms of passive films, thereby expediting the required optimization.

Acknowledgements

The support for this study from the US Army Communications-Electronics Command Center (CECOM), University of Wisconsin, and Argonne National Laboratory is gratefully acknowledged. Helpful suggestions from Prof. F. Mansfeld are also gratefully acknowledged.

References

[1] H. Nakahara, A. Masias, S.Y. Yoon, T. Koike, K. Takeya, Proceedings of the 41st Power Sources Conference, vol. 165, Philadelphia, June 14–17, 2004.
[2] H. Nakahara, S.Y. Yoon, T. Piao, S. Nutt, F. Mansfeld, J. Power Sources 158 (2006) 591–599.
[3] H. Nakahara, S.Y. Yoon, S. Nutt, J. Power Sources, doi:10.1016/j.jpowsour.2005.09.050.
[4] M. Inaba, Z. Shiroya, Y. Kawatate, A. Funabiki, Z. Ogumi, J. Power Sources 68 (2) (1997) 221–226.
[5] S.-K. Jeong, M. Inaba, Y. Iriyama, T. Abe, Z. Ogumi, Electrochim. Acta 47 (2002) 1975–1982.
[6] R. Mogi, M. Inaba, Y. Iriyama, T. Abe, Z. Ogumi, J. Power Sources 108 (2002) 163–173.
[7] D. Aurbach, E. Zinigrad, Y. Cohen, H. Teller, Solid State Ionics 148 (2002) 405–416.
[8] D. Aurbach, I. Weissman, A. Zaban, P. Dan, Electrochim. Acta 45 (1999) 1135–1140.
[9] D. Aurbach, A. Zaban, Y. Gofer, Y.E. Ely, I. Weissman, O. Chusid, O. Abramson, J. Power Sources 54 (1995) 76–84.
[10] Z. Ogumi, A. Sano, M. Inaba, T. Abe, J. Power Sources 97–98 (2001) 156–158.
[11] K. Xu, S. Zhang, B.A. Poese, T.R. Jow, Electrochem. Solid-State Lett. 5 (1) (2002) A259–A262.
[12] K. Xu, S. Zhang, T.R. Jow, W. Xu, C.A. Angell, Electrochem. Solid-State Lett. 5 (1) (2002) A26–A29.
[13] K. Xu, S. Zhang, T.R. Jow, Electrochem. Solid-State Lett. 6 (6) (2003) A117–A120.
[14] Y. Kang, W. Lee, D.H. Suh, C. Lee, J. Power Sources 119–121 (2003) 448–453.
[15] I.J. Lee, G.S. Song, W.S. Lee, C. Lee, J. Power Sources 114 (2003) 320–329.
[16] M. Shibata, T. Kobayashi, R. Yosomiya, M. Seki, Eur. Polym. J. 36 (2000) 485–490.
[17] Z. Zhang, S. Fang, Electrochim. Acta 45 (2000) 2131–2138.

[18] Z. Wang, M. Ikeda, N. Hirata, M. Kubo, T. Ito, O. Yamamoto, J. Electrochem. Soc. 146 (6) (1999) 2209–2215.
[19] B. Oh, D. Vissers, Z. Zhang, R. West, H. Tsukamoto, K. Amine, J. Power Sources 119–121 (2003) 442–447.
[20] A.M. Andersson, Dissertation for the Degree of Doctor of Philosophy, Uppsala University, 2001.
[21] A.M. Andersson, K. Edstorm, J. Eletrochem. Soc. 148 (2001) A1100–A1109.
[22] A.M. Andersson, M. Herstedt, A.G. Bishop, K. Edstrom, Electrochim. Acta 47 (2002) 1885–1898.
[23] D. Aurbach, Nonaqueous Electrochemistry, Marcel Dekker, New York, 1999.
[24] D. Aurbach, A. Zaban, Y. Ein-Eli, I. Weissman, O. Chusid, B. Markovsky, M. Levi, A. Shechter, E. Granot, J. Power Sources 68 (1997) 91.
[25] A. Kominato, E. Yasukawa, N. Sato, T. Ijuuin, H. Asahina, S. Mori, J. Power Sources 68 (1997) 471.
[26] C.S. Wang, A.J. Appleby, F.E. Little, Electrochim. Acta 46 (2001) 1793.
[27] N. Hiroyoshi, S. Kuroiwa, H. Miki, M. Tsunekawa, T. Hirajima, Hydrometallurgy 74 (2004) 193.
[28] K. Abe, H. Yoshitake, T. Kitakura, T. Hattori, H. Wang, M. Yoshio, Electrochim. Acta 49 (26) (2004) 4613.
[29] M.-S. Wu, P.-C.J. Chiang, J.-C. Lin, J.-T. Lee, Electrochim. Acta 49 (2004) 4379.
[30] M.S. Michael, S.R.S. Prabaharan, J. Power Sources 136 (2004) 250.
[31] S.-H. Choi, J. Kim, Y.-S. Yoon, Electrochim. Acta 50 (2–3) (2004) 547.
[32] C.H. Chen, J. Liu, M.E. Stoll, G. Henriksen, D.R. Vissers, K. Amine, J. Power Sources 128 (2004) 278.
[33] J.-H. Kim, C.W. Park, Y.-K. Sun, Solid State Ionics 164 (2003) 43.
[34] Z.P. Guo, S. Zhong, G.X. Wang, H.K. Liu, S.X. Dou, J. Alloys Compd. 348 (2003) 231.
[35] S.S. Zhang, T.R. Jow, J. Power Sources 109 (2002) 458.
[36] S. Zhang, P. Shi, Electrochim. Acta 49 (2004) 1475.
[37] Z. Ogumi, T. Abe, T. Fukutsuka, S. Yamate, Y. Iriyama, J. Power Sources 127 (2004) 72.
[38] S. Komaba, T. Itabashi, B. Kaplan, H. Groult, N. Kumagai, Electrochem. Commun. 5 (2003) 962.
[39] J. Yao, G.X. Wang, J.-H. Ahn, H.K. Liu, S.X. Dou, J. Power Sources 114 (2004) 292.
[40] M. Nookala, B. Kumar, S. Rodrigues, J. Power Sources 111 (2002) 165.
[41] Y.-K. Choi, K.-I. Chung, W.-S. Kim, Y.-E. Sung, S.-M. Park, J. Power Sources 104 (2002) 132.
[42] S.B. Lee, S.-I. Pyun, Carbon 40 (2002) 2333.
[43] B. Jin, J.-U. Kim, H.-B. Gu, J. Power Sources 117 (2003) 148.
[44] C.R. Yang, J.Y. Song, Y.Y. Wang, C.C. Wan, J. Appl. Electrochem. 30 (2000) 29.
[45] Y.C. Chang, J.H. Jong, G.T.K. Fey, J. Electrochem. Soc. 147 (2000) 2033.
[46] Y.C. Chang, H.J. Sohn, J. Electrochem. Soc. 147 (2000) 50.
[47] M. Holzapfel, A. Martinent, F. Alloin, B. Le Gorrec, R. Yazami, C. Montella, J. Electroanal. Chem. 546 (2003) 41.
[48] T. Piao, S.M. Park, C.H. Doh, S.I. Moon, J. Electrochem. Soc. 146 (1999) 2794.
[49] F. Prieto, I. Navarro, M. Rueda, J. Electroanal. Chem. 550–551 (2003) 253.
[50] N. Hiroyoshi, S. Kuroiwa, H. Miki, M. Tsunekawa, T. Hirajima, Hydrometallurgy 74 (2004) 193.
[51] S. Yoon, H. Kim, S.-M. Oh, J. Power Sources 94 (2001) 68.
[52] J.R. MacDonald, Impedance Spectroscopy: Emphasizing Solid Materials and Systems, John Wiley & Sons, New York, 1987.
[53] J. Bisquert, A. Compte, J. Electroanal. Chem. 499 (2001) 112.
[54] Y.O. Kim, S.M. Park, J. Electrochem. Soc. 148 (2001) A194.
[55] E. Basrsoukov, J.H. Kim, C.H. Yoon, H. Lee, J. Electrochem. Soc. 145 (1998) 2711.
[56] J.-S. Kim, Y.-T. Park, J. Power Sources 91 (2000) 172.
[57] M.W. Wagner, Electrochim. Acta 10 (1997) 1623.
[58] V. Doge, J. Dreher, G. Hambitzer, IEEE 0-7803-2459-5/95 (1995).
[59] S. Buller, M. Thele, R.W. De Doncker, IEEE 0-7803-0/03 (2003).
[60] I. Uchida, M. Mohamedi, K. Dokko, M. Nishizawa, T. Itoh, M. Umeda, J. Power Sources 97–98 (2001) 518.
[61] R. M. Spotnitz, IEEE 0-7803-5924-0/00 (2000).
[62] M.J. Issacson, N.A. Torigoe, R.P. Hollandsworth, IEEE 0-7803-4098-1/98 (1998).
[63] J. Conard, V.A. Nalivoma, D. Guerard, Mol. Cryst. 245 (1994) 25.
[64] K. Tanaka, M. Ata, H. Kimura, H. Imoto, Bull. Chem. Soc. Jpn. 67 (1994) 2430.
[65] L.J. Krause, W. Lamanna, J. Summerfield, M. Engle, G. Korba, R. Loch, J. Power Sources 68 (1997) 320.
[66] K. Naoi, M. Mori, Y. Narupka, W.M. Lamanna, R. Atanasoski, J. Electrochem. Soc. 146 (1999) 462.
[67] S.-Y. Yoon, H. Nakahara, Z. Zhang, Q. Wang, K. Amine, R. West, H. Tsukamoto, Proceedings of the Second International Conference on Polymer Batteries and Fuel cells, Abstract No. 121, Las Vegas, USA, June 12–17, 2005.